A strategy to assess aerosol direct radiative forcing of climate using satellite radiation measurements

Yoram J. Kaufman[1] and Didier Tanré[2]

1. NASA Goddard Space Flight Center, code 913, Greenbelt MD 20771; Tel (301) 614-6189; E-mail kaufman@climate.gsfc.nasa.gov

2. Laboratoire d'Optique Atmospherique, CNRS, Université de Sciences et Techniques de Lille, Villeneuve d'Ascq, France.

ABSTRACT

Atmospheric aerosols have a complex internal chemical composition and optical properties. Therefore it is difficult to model their impact on redistribution and absorption of solar radiation, and the consequent impact on atmospheric dynamics and climate. The use in climate models of isolated aerosol parameters retrieved from satellite data (e.g. optical thickness) may result in inconsistent calculations, if the model assumptions differ from these of the satellite retrieval schemes. Here we suggest a strategy to assess the direct impact of aerosol on the radiation budget at the top and bottom of the atmosphere using satellite and ground based measurements of the spectral solar radiation scattered by the aerosol. This method ensures consistent use of the satellite data and increases its accuracy. For

anthropogenic aerosol in the fine mode (e.g. biomass burning smoke and urban pollution) consistent use of satellite derived optical thickness can yield the aerosol impact on the spectral solar flux with accuracy an order of magnitude better than the optical thickness itself. For example, a simulated monthly average smoke optical thickness of 0.5 at 0.55 μm (forcing of 40-50 W/m^2) derived with an error of 20%, while the forcing can be measured directly with an error of only 0-2 W/m^2. Another example, the effect of large dust particles on reflection of solar flux can be derived three times better than retrievals of optical thickness. Since aerosol impacts not only the top of the atmosphere but also the surface irradiation, a combination of satellite and ground based measurements of the spectral flux, can be the most direct mechanism to evaluate the aerosol effect on climate and assimilate it in climate models. The strategy is applied to measurements from SCAR-B and the Tarfox experiments. In SCAR-B aircraft spectral data are used to derive the 24 hour radiative forcing of smoke at the top of the atmosphere of $\Delta F_{24hr}/\Delta\tau = -25\pm5$ w/m^2. Ground based data give forcing at the surface of $\Delta F_{24hr}/\Delta\tau = -80\pm5$ W/m^2. In TARFOX a mixture of maritime and regional pollution aerosol resulted in a varied forcing at the top of the atmosphere, $\Delta F_{24hr}/\Delta\tau$, between -26 W/m^2 and –50 W/m^2 depending on mixture of coarse and accumulation modes, for Angstrom exponents of 1.0 and 0.2 respectively.

1. Introduction

Aerosol impact on solar radiation at the top of the atmosphere is defined as the change in the ability of the Earth system to reflect sunlight to space due to the presence of aerosol. Aerosol impact at the surface is defined in a similar way but refers to the change in the solar radiation reaching the surface. Aerosol direct radiative forcing of climate is the change in the radiative impact due to change in the concentration or properties of man-made aerosol. For simplicity we shall call the change in the reflected or transmitted solar flux due to the presence of aerosol, radiative forcing. Measurements in locations minimally affected by humans may determine the background natural aerosol that can be used to deduce the anthropogenic forcing [Kaufman et al., 2001]. In recent years, several studies pointed to the potential of aerosol to counter balance some of the greenhouse forcing, at least above the industrial regions, by reflecting solar radiation to space and changing the radiation balance at the top of the atmosphere [e.g. Charlson et al., 1992; Hobbs et al 1997]. However, climate models [Hansen et al., 1997] and recent field measurements [Satheesh and Ramanathan, 2000] show that understanding radiative forcing at the top of the atmosphere is not enough to represent the aerosol effect on climate. Absorbing aerosol, e.g. biomass burning [Martins et al., 1998], regional pollution over the Indian Ocean [Satheesh et al., 1999] and dust [Alpert et al., 1998] can affect atmospheric heating rates, evaporation and cloud formation; thus affecting climate even without directly changing the energy balance at the top of the atmosphere. In essence aerosol reduces surface insolation by reflecting radiation to space (forcing at the top of the atmosphere) and by absorbing solar radiation in the atmospheric

column. Thus determination of the aerosol forcing at the top of the atmosphere, when combined with determination of radiative forcing at the surface, reveals the aerosol effect on the energy redistribution in the atmosphere and at the surface [Satheesh and Ramanathan, 2000].

Present assessments of the aerosol radiative forcing at the top of the atmosphere are made with the help of global models that use knowledge of the aerosol sources, properties and evolution in the atmosphere [e.g. Kiehl and Briegleb, 1993; Hansen et al., 1997; Tegen et al., 1996]. The models are evaluated against satellite and ground based measurements of the global distribution of the aerosol optical thickness [Tegen et al., 1996]. However aerosol particles are very complex chemical and physical constituents of the atmosphere. Every aerosol particle may differ from another due to differences in the microchemical history of the particle. Its complex internal structure and variable spatial distribution cannot be measured with enough detail. Simplifying assumptions are needed to introduce aerosols in the models. This introduces a significant error in modeling aerosol forcing. If the models are initiated or evaluated using optical thickness maps derived from satellites [Husar et al., 1997; Nakajima and Higurashi, 1998; Michshenko et al., 1999], differences between the assumptions used to derive the optical thickness and the aerosol description in the models can yield inconsistent flux calculations.

The global distribution of the aerosol spectral optical thickness and other properties are derived, in the case of the MODIS instrument, launched on the Terra satellite in Dec. 1999, from measurements of the spectral radiation field over the ocean [Tanre et al., 1997, 1999] and land [Kaufman et al., 1997; Chu et al., 1998]. The

derivation requires a set of assumptions and simplifications to derive the aerosol properties. E.g. that particles are spherical and homogeneous, that the refractive indices are known and that the size distribution can be described by a two modal log-normal distribution. Similar assumptions are made in the analysis of data from other satellites; see review by King et al., [1999]. Climate models, that compute the aerosol radiative forcing, also supplement the present knowledge with set of assumptions about the aerosol properties and their evolution. These two sets of assumptions are not necessarily consistent. Thus large errors in the estimate of the aerosol radiative forcing can be anticipated. A strategy that is based on a consistent set of assumptions between the inversion of the aerosol properties from the satellite data and climate models, can provide the best tool to assess the aerosol direct forcing of climate. A direct method to achieve this consistency is to evaluate or assimilate the climate models using measurements of the aerosol impact on the spectral radiative fluxes reflected to space and reaching the surface. In this paper we present a sensitivity study to investigate the accuracy in the use of satellite spectral radiances, as available presently from MODIS instrument to derive the spectral flux reflected to space. In a different paper we assess the use of AERONET sky measurements to derive the aerosol effect on the surface irradiation.

2. MODIS aerosol measurements

The MODIS instrument was launched on the Terra mission for 10:30 am global observations. It has 8 spectral channels in the solar region that can be used to investigate the aerosol radiative impact: 0.41, 0.47, 0.55, 0.66, 0.86, 1.2, 1.65, 2.13 μm.

The instrument is scanning the earth perpendicular to its polar orbit in a wide range of observation view angles (±70°). Measurements of the spectral reflective properties of the Earth and atmosphere are expected to be within accuracy of 2% and a better spectral and temporal precision. Over the dark oceans the information is used to derive the daily global aerosol spectral optical thickness and the aerosol size distribution [Tanré et al., 1997; 1999]. The size distribution is derived assuming that it is composed from an accumulation and coarse modes. The modes are selected from a look-up table and their concentrations are adjusted to fit the spectral radiance. The look-up table is constructed for (30) different combinations of aerosol size distribution, assuming spherical homogeneous particles with preprescribed refractive index. This strategy is based on the information content of the spectral signal that allows no more than three independent pieces of information to be derived from the MODIS data [Tanré et al., 1996], and extensive measurements of the aerosol properties [Remer et al., 1998, Remer and Kaufman, 1998; Tanré et al., 2000]. Errors in these assumptions, will result in errors in the derived optical thickness, though note that preflight validation effort showed an excellent performance [Tanré et al., 1999]. Since the scattered light is sensitive mainly to the scattering optical thickness, the reported total aerosol optical thickness is affected by uncertainty in the single scattering albedo. Presently no aerosol information is derived over the bright glint region (glint angle <40°). Over the land the aerosol optical thickness is derived in the red (0.66 μm) and blue (0.47μm) channels where vegetated land is dark, and the ratio of the accumulation to coarse mode is estimated [Kaufman et al., 1997a; Chu et al., 1998]. New techniques to estimate the aerosol

single scattering albedo from multispectral data are being developed [Kaufman et al., 2000] based on old principles [Fraser and Kaufman 1985; Kaufman, 1987], but they are still in experimental stages of development.

Here we propose to use the MODIS measurements of the spectral radiances not only to derive the aerosol optical thickness and size distribution, but also to derive directly the aerosol impact on the spectral radiation flux. We shall show that in many cases the flux can be derived even more accurately than the optical thickness itself, due to its physical similarity to radiance. In essence, since the flux is the two dimensional angular integral on the radiance, the aerosol properties are needed only to extrapolate the radiance from a particular direction or set of directions (in case of monthly means) to the integrated flux value.

3. Sensitivity study

How accurately can MODIS be used to derive the aerosol effect on the spectral flux reflected to space? To answer this question we compute the error in the derivation of the fluxes from the radiation field measured from space over the ocean, in the presence of uncertainties in MODIS calibration, uncertainty in surface reflectivity (error in wind speed of 2 m/s) and errors in the assumed aerosol model. Monthly means are derived for each latitude zone. In each mean the range of view angles that is observed by MODIS is used. Monthly averaging decreases the sensitivity of the derived flux to the aerosol model and increases its accuracy, due to averaging on a range of scattering angles. Figure 1 shows the range of scattering

angles used in the analysis for each latitude zone. The calculations are for the Terra orbit, over a period of one month during the equinox (sun located over the equator). The maximal range of scattering angles is over the tropical regions, except of a central range of angles that is missing due to the need to avoid the solar glint. The wider the range of scattering angles used in the flux derivation, the less dependent the angularly integrated flux is on the aerosol model. In the extreme case, if all relevant scattering angles would have been presented, the measured radiation field would have included all the scattering information, and the calculation of the flux would be equivalent to a weighted integral on the measured radiation, with no sensitivity to the aerosol model.

The main results of the sensitivity study for observations over the ocean are shown in Fig. 2, 3 and Table 1. The error in the aerosol optical thickness, τ, at 0.55 μm and the derived impact of aerosol on the spectral flux, ΔF_{aer}, at 0.55 μm, 0.86 μm and 1.65 μm are plotted in Fig. 2, for accumulation mode and coarse mode aerosol. ΔF_{aer} is the difference in the upward spectral flux with and without the aerosol. It is normalized by the incoming solar radiation per unit area of the surface ($F_o\mu_o$), where μ_o is cosine of the solar zenith angle. The data points are sorted as a function of latitude. Three kinds of errors are included:

- Spectral calibration errors (3% at 0.55 μm, 2.5% at 0.66 μm, 2% at 0.86 μm, 1.5% at 1.24 μm, 1% at 1.64 μm, and 0% at 2.1 μm).

- Aerosol model errors – difference between the simulated aerosol properties and the look-up table used in the inversion scheme of Tanré et al. [1997] of modal size (of ~10%) and refractive index (of 0.1).
- Error in the surface reflectance due to error in the wind speed of 2m/s.

Note that the spectral dependence of the calibration errors result in an error not only in the absolute magnitude of the radiances and fluxes but also in the derived aerosol size distribution. For the accumulation mode, the combined result of errors in calibration, wind speed and model errors cause an order of magnitude smaller error in ΔF_{aer} than in the optical thickness (top of Fig. 2 and Table 1). This is important in the observation of the aerosol forcing since both in the case of urban pollution and biomass burning aerosol, the main impacts on climate is from particles in the accumulation mode (this is not the case for dust). The coarse mode (e.g. in case of dust) shows a different behavior (bottom of Fig. 2). Here the impact of inaccuracy in the model (mainly the refractive index) on the optical thickness and on ΔF_{aer} are large, though the errors in the flux ~20% are much smaller than in the optical thickness 50%. The error in the optical thickness in this simulation is much larger than the actual errors found in validation of the MODIS aerosol products (Tanre et al., 1999; Remer et al., 2001) and is used for illustration only.

What is the impact of these errors on the instantaneous solar radiative budget at the top of the atmosphere? We estimate the aerosol impact on the integrated solar flux for the 10:30 satellite equatorial crossing and a tropical atmosphere model using the at 0.55, 0.86 and 1.64 μm. The spectrum was

subdivided and an amount of transmitted solar energy was associated with each spectral wavelength. The resulting aerosol effect on reflection of the integrated spectral radiation to space, and the errors in the estimate are plotted in Fig. 3 for the accumulation mode and coarse mode aerosol. The accumulation mode reflects 42-54 W/m^2 to space, depending on latitude, with an error of only 0-2 W/m^2. The coarse mode reflects 10-20 W/m^2 with an error of 4-7 W/m^2. Though we still have a major problem of estimating the radiative forcing of dust using this method, the ability to estimate the impact of regional pollution aerosol or biomass burning smoke on climate can be done very accurately. We did not include error in the single scattering albedo in the sensitivity study. But since both the effect of aerosol on the radiance and the flux are to first order proportional to the single scattering albedo, while the optical thickness is not dependent on it, again the error in ΔF_{aer} will be much smaller than the error in τ.

4. Analytical motivation

The small sensitivity of the derived spectral fluxes on the assumed aerosol properties can be explained using single scattering approximation. The aerosol contribution to the normalized radiance at the top of the atmosphere for zero surface reflectance is given by:

$$\rho^*_{aer}(\tau) = \omega_o \tau P/(4\mu\mu_o) \qquad (1)$$

where, ω_o is the aerosol single scattering albedo, τ is the aerosol optical thickness, P the scattering phase function, μ and μ_o cosines of the view and solar zenith angle respectively.

The corresponding normalized fluxes are:

$$\Delta F_{aer}(\tau) = \omega_o \tau \beta / \mu_o \quad (2)$$

where, β is the aerosol backscattering fraction. Therefore:

$$\Delta F_{aer}(\tau) / \rho^*_{aer}(\tau) = 4\mu\beta/P \quad (3)$$

Independent of the aerosol loading (τ) and single scattering albedo, ω_o. The backscattering function, β, is an integral on part of the angular range of P. Therefore averaging the ratio in (3) over the view direction, during a month of observations will further decrease the dependence on the aerosol properties.

5. Strategy based on satellite measurements of the spectral fluxes

Are measurements of the spectral flux reflected to space the best approach for assessment of the aerosol direct forcing? There are four main approaches that can be used for the assessment of aerosol direct radiative forcing at the top and bottom of the atmosphere. In the following we review the pros and cons of these approaches. We discuss only aerosol forcing in cloud free conditions. Aerosol asserts also direct radiative forcing when present above clouds [Boucher and Anderson 1995; Hansen et al., 1997] and under thin clouds.

1. General Circulation Model approach: The general circulation model is used to compute transport of the aerosol and to compute the atmospheric conditions that affect the aerosol properties. Aerosol sources or aerosol precursors are introduced (e.g. SO_2 for sulfate aerosol – Kiehl and Briegleb, 1993) and the radiative forcing is calculated (e.g. for dust Tegen et al., 1996).

The drawback of this approach is the complex chemical and physical properties of every single aerosol particle, and the interaction between aerosol precursors from different chemical sources. For example, the difference between a mixture of 90% organic aerosol with10% of black carbon in an external mode (the two are separate aerosol particles in the atmosphere) vs. internal mode (the two are mixed inside the same particle) can generate a factor of 3 difference in the ability of the aerosol to absorb solar radiation [Martins et al., 1998; Jacobson, 2001], and therefore can change the magnitude and even the direction of the aerosol forcing. The interaction of hygroscopic aerosol with water vapor depends on the particle chemistry and on the spatial variability of humidity. Haywood et al. [1997] studied this process using two climate models with different spatial resolutions and concluded that the higher spatial resolution can increase the direct forcing by some 80%, due to the nonlinear effect of relative humidity on the particle growth. Another issue is the inclusion of realistic surface spectral reflectance. The high spatial and temporal variation of the surface reflective properties over the land is difficult to be captured by climate models. The aerosol forcing over the land depends on the surface reflectivity. Over vegetation, that is

dark in the visible part of the spectrum, the effect of aerosol in the accumulation mode is strong. Over bright soils the effect is weak or negative (Fraser and Kaufman 1985). Before we have detailed realistic models of the aerosol formation and evolution and its interaction with the environment, global circulation models have to be limited to sensitivity studies rather than real assessment of the aerosol forcing.

2. Aerosol assimilation using direct aerosol measurements: A second approach can build on the first one, but adjust the GCM calculated aerosol field using daily measurements of the aerosol optical thickness. Optical thickness is derived from satellite data and from the ground-based sunphotometer network. This approach will work better than the first one, since the optical thickness is sensitive to the aerosol composition and interaction with water vapor, and therefore will correct for some of the inadequacies of the aerosol climatology in the climate model. However the sensitivity of the optical thickness to the aerosol properties is not the same as that of the radiative fluxes. Fluxes are the product of the aerosol optical thickness with the backscattering ratio and the single scattering albedo (Eq. 2). The later two parameters are sensitive to the aerosol properties differently than the optical thickness.
3. Aerosol assimilation using spectral fluxes derived from remote sensing: Here we overcome the last problem by deriving directly the spatially and temporally variable impact of aerosol on the spectral solar energy redistribution. Therefore take advantage of the fact that fluxes are better related to the physics of the

problem. Fluxes are independent of the satellite orbit information, and therefore easier to implement than radiance. The question arises: why to use MODIS monthly averaged fluxes rather than CERES data. The CERES instruments on the morning and afternoon EOS missions (Terra and Aqua) have a better angular representation than MODIS to derive the changes in the reflected solar flux. Due to the specific measurement technique CERES data have much better calibration than MODIS, with an error of 0.2%. CERES provides flux integrated on the entire solar spectrum. However CERES data mix the visible part of the spectrum, which is very sensitive to the effects of accumulation mode aerosol and the near-IR part of the solar spectrum that is not. Over land, which is much brighter in the near-IR than in the visible, this can generate substantial errors due to variability of surface cover and water vapor absorption. Fig. 4 demonstrates this effect using measurements by the AVIRIS spectrometer flown in the SCAR-B experiment in a biomass burning region on the ER-2 (Kaufman et al., 1998). Here the apparent reflectance of vegetation with smoke above it is plotted as a function of wavelength (λ). For $\lambda<0.7$ the vegetation is dark and most of the signal is due to aerosol. In this spectral range it is easier to derive the aerosol forcing. For $\lambda>0.7$ the surface is bright, the aerosol signal is much smaller and depends on its single scattering albedo (Fraser and Kaufman, 1985). Small variation in the surface reflectance in the near-IR, may overshadow the aerosol impact on the integrated reflected solar flux. Additional advantage of MODIS is the spatial resolution of 0.5 km in the solar spectrum vs. 20 km of CERES. The higher resolution will help distinguish between broken clouds and aerosol to measure the aerosol

forcing in partially cloudy conditions. The MODIS spectral measurements, extending throughout the solar spectrum, with moderate spatial resolution, are therefore most suitable to measure the aerosol radiative forcing. The need for monthly averaging the MODIS data may be avoided if MODIS data are combined with the along track measurements of MISR on Terra (Kahn et al., 1998) or the two dimensional angular distribution of POLDER planned to fly in the same orbit with MODIS on Aqua (Boucher and Tanré, 2000). The assimilated data can be used to interpolate the aerosol field into cloudy regions to calculate the direct forcing there and using data on the aerosol absorption derive the forcing at the surface.

4. Combination of satellite and ground based measurements

The MODIS measurements at the top of the atmosphere can be complemented by spectral flux measurements from the surface. A combination of ground based and spaceborne measurements of the integrated reflected and transmitted solar flux was published recently by Satheesh and Ramanathan [2000]. The AERONET network of sky/sun radiometers [Holben et al., 1998; 2001] can be used to derive the spectral flux reaching the surface [Kaufman et al., 2000a]. An example is given in section 6. However ground based measurements are limited in their spatial extent. Since the reduction in the spectral solar radiation reaching the surface is due to backscattering to space (measured from satellite) and due to absorption of sunlight, represented by the single scattering albedo and total aerosol optical thickness, it may be estimated from the satellite data. Methods to evaluated aerosol absorption with satellite data were published

[Kaufman, 1987] and are being further developed [Kaufman et al., 2000b]. Therefore it may be possible to establish the aerosol effect on radiative budget at the top and bottom of the atmosphere using satellite data alone, and more accurately using a combination of satellite and ground based network of radiometers in locations where these are available. Aerosol assimilation models together with satellite measurements can be used to extend the result into cloud regions

6. Example of implementation to biomass burning

To simulate the use of satellite data to estimate the effect of aerosol on backscattering solar radiation to space, we use again the AVIRIS spectral data. The method is based on two principles: (1) Smoke is visible in the short solar wavelengths and transparent in the mid-IR (see Fig. 4). (2) Surface reflectance in the visible part of the spectrum are highly correlated to the surface reflectance in the mid-IR [Kaufman et al., 1997b]. Therefore images in the long wavelengths (1.65 and 2.1 μm) can be used to estimate the surface + molecular scattering contribution to the flux in the short wavelengths: 0.4-0.7 μm range. We used smoke free locations to find the following empirical relationship between the surface reflectance at 1.65 and 2.13 μm and the AVIRIS radiance integrated on the AVIRIS spectrum in the 0.4-0.7 μm range (see Fig. 5):

$$\pi L^{s}_{0.4\text{-}0.7\mu m} = 19 + 291 \cdot \rho_{2.13} - 44 \cdot \rho_{1.65} (W/m^2) \qquad (4)$$

The aerosol effect on reflected sunlight $\pi\Delta L_{0.4\text{-}0.7\mu m}$ is derived from the difference between the actual integral on the measured spectral radiance from AVIRIS $\pi L_{0.4\text{-}0.7\mu m}$ and the estimated surface+molecular scattering contribution:

$$\pi\Delta L_{0.4\text{-}0.7\mu m} = \pi L_{0.4\text{-}0.7\mu m} - \pi L^{s}_{0.4\text{-}0.7\mu m} \quad (7)$$

The results, indicating the aerosol radiative impact at nadir, are plotted in Fig. 6 (top panel) for several locations. The data are fitted with a smoke aerosol model [Remer et al., 1998] that is then used to convert the measured radiance difference $\pi\Delta L_{0.4\text{-}0.7\mu m}$ to the instantaneous flux for unit optical thickness: $\Delta F_{0.4\text{-}0.7\mu m}/\Delta\tau = 70$ W/m^2. Note that since AVIRIS observations are only at nadir, the choice of the model to convert from the radiance to flux is much more important than in the case of MODIS with multiple view directions of observations in a given month. Since this flux is of reflected solar radiation, the corresponding radiative forcing is negative: -70 W/m^2. The forcing for 0.7-2.1 μm is insignificantly different from zero, due to a balance between an increase in the backscattering to space for λ<0.8 μm and decrease for λ >0.8 μm (see bottom panel of Fig. 6). For a wide range of solar zenith angles (Fig. 7) we found forcing of -50 to -70 W/m^2 $28°\leq\theta_o\leq67°$, and averaged on 24 hours: $\Delta F_{24hr}/\Delta\tau = -25\pm5$ W/m^2. We assumed equal probability of solar zenith angles in the calculations. This is similar to the measurements in INDOEX [Satheesh and Ramanathan 2000].

The effect of aerosol on diffuse solar radiation reaching the Earth surface is derived from principal plane radiances measured by the AERONET federated global

network of sun/sky radiometers. These autonomous instruments, measure the direct transmission of sunlight to the surface and the sky brightness in the almucantar plane and the principal plane passing through the sun [Holben et al., 1998]. Though the principal plane is only one line in the sky, it contains all the scattering angles present in the sky. Since all the physical and chemical parameters that determine the optical properties of the aerosol and the sky radiance are only function of the scattering angle, we should be able to reconstruct accurately the sky brightness from the principal plane measurements. The advantage of fluxes derived from the radiance in the principal plane, is that it is easier to avoid scattered clouds and derive the fluxes in their presence. In a recent paper [Kaufman et al., 2000a] we showed that the diffuse flux can be derived from the principal plane measurements with an additional error of 2.5%, smaller than the calibration errors of 5% in the radiance.

To apply the method to measurements, a cloud screening technique was developed based on the smoothness of the angular distribution of the sky data. Fig. 8 shows results of the measurements in Alta-Floresta, Brazil and compares them with smoke model of Remer et al. (1998). Sky radiance increases with the smoke optical thickness, reaching a maximum, then decreases due to the overwhelming effects of smoke absorption and backscattering to space. The diffuse solar fluxes derived from the AERONET radiometer fit the model for optical thickness less than 0.6 (for which the model was derived) and are higher than the model for higher optical thicknesses. AERONET data collected in Cuiaba, Brazil were compared with the model and with shadow band fluxes. The results show that the model correlates very well with the measurements (r=0.98). Aerosol forcing at the surface - the difference in the total solar

flux reaching the surface for an atmosphere with and without aerosol, when integrated on the solar spectrum, gives smoke forcing of $\Delta F_{24hr}/\Delta\tau$ = -80±5 W/m^2, assuming equal distribution of solar zenith angles across the day. This is also similar to the INDOEX measurements, unsurprisingly since the aerosol single scattering albedo is similar in both cases [Hobbs et al., 1997; Satheesh et al., 1999].

7 Example of implementation to regional pollution aerosol

In the Tarfox experiment (Russell et al., 1999) spectral imaging of the radiance at the top of the atmosphere (20 km height) over the ocean was conducted using the MODIS Airborne Simulator (MAS). The conditions included maritime air and regional pollution aerosol. The spectral optical thicknesses derived from the spectral MAS data are plotted in Fig. 9 (Tanré et al., 1999). The Angstrom exponent varied from 0.2 (predominantly large particles) to 1.0 (mixed small and large particles). The MAS spectral radiances are also used to derive the aerosol optical properties and to calculate the corresponding flux at the top of the atmosphere. The spectral radiative forcing due to the aerosol, normalized to the incoming solar flux F_o and to unit optical thickness at 0.55 μm:

$$\Delta f/\Delta\tau_{0.55} = \Delta F(\lambda)/(F_o\mu_o\Delta\tau_{0.55}) ,$$

is plotted in Fig. 9. We used the spectral fluxes to integrate on the solar spectrum and on the daily cycle. Since the measurements were conducted for specific solar zenith angle of 67°, we assume that the reflected flux at any other solar zenith angle can be expressed by:

$$\Delta F(\lambda, \mu^*_o)/\Delta\tau_{0.55} = [\Delta f(\mu_o)/\Delta\tau_{0.55}]F_o(\lambda)\mu^*_o[1-\exp(-\tau_\lambda/\mu^*_o)]/[1-\exp(-\tau_\lambda/\mu_o)]$$

Here we use the single scattering approximation that the scattered flux varies with the solar zenith angle as $\mu_o[1-\exp(-\tau_\lambda/\mu_o)]$

where μ^*_o is cosine of the new solar zenith angle and μ_o is cosine of 67°.

The 24 hour average aerosol radiative forcing, for the lowest Angstrom expenent of 0.2 is $\Delta F_{24hr}/\Delta\tau$ = -50 W/m^2, significantly higher than the value found from biomass burning. This is the result of the higher single scattering albedo (0.96 instead of 0.86) and the small Angstrom exponent that results in significant forcing for spectral range larger than 1 μm. For Angstrom exponent of 1.0, the radiative forcing of $\Delta F_{24hr}/\Delta\tau$ =-26 W/m^2, similar to that of biomass burning. For comparison on different days Hignett et al. (1999) and Russell et al. (1999) measured the upward flux from the aircraft, indicating the difficulty of doing so. They found $\Delta F_{24hr}/\Delta\tau$ between -25 W/m^2 and -60 W/m^2.

8. Conclusions

We showed that the use of aerosol effect on the spectral fluxes derived from satellite data can be a more accurate determinant of the aerosol forcing at the top of the atmosphere than the optical thickness. Combination of satellite data and ground based measurements, or remote sensing of aerosol absorption from the satellite data can be used to study the aerosol forcing at the surface and deduce the heating rates in the atmosphere. A summary of the sensitivity study for five latitude zones is given in Table 1. It demonstrates that the errors in the derived contribution of the aerosol

fine mode to the flux is much smaller than the error in the optical thickness. Since the fine mode is responsible for the anthropogenic impact on climate of urban pollution and biomass burning, the small errors show that measurements of the effect of aerosol on the flux is a good measure of its radiative forcing at the top of the atmosphere. As an example, a strategy for the assessment of the aerosol direct radiative forcing can include the following steps:

1. Using MODIS global spectral data determine the distribution of aerosol loading and properties and the distribution of the aerosol contribution to the reflection of the spectral flux at the top of the atmosphere.
2. Using ground based measurements of the sky irradiance, estimate the aerosol impact on the spectral aerosol flux reaching the surface.
3. Using satellite derivation of the aerosol optical thickness and single scattering albedo estimate the aerosol absorption of sunlight and the radiative forcing at the surface. Evaluate and adjust the results using the ground based measurements.
4. Simulate the aerosol global distribution and aerosol forcing using most updated aerosol transport models.
5. Adjust the aerosol representation in the model and the aerosol radiative impacts using the MODIS and ground based measurements of the aerosol fluxes.
6. Use the model to interpolate the aerosol field and the aerosol forcing in the cloudy regions. Use the models to extrapolate the aerosol field and forcing to regions where the aerosol concentration is too small for reliable detection.

7. Check for consistency against total monthly flux measurements at the top of the atmosphere by CERES and at the ground by Pyranometers.
8. Subtract the contribution of the natural aerosol to the aerosol impact by measuring the aerosol properties in remote undisturbed sites.

Remote sensing of the aerosol radiative forcing will be enhanced at the end of 2000 with the launch of EOS-Aqua with a second MODIS instrument for a second daily measurement at 1:30 PM. It will be farther enhanced with the launch at 2003 of the Picasso mission with a two channel lidar for measurements of the aerosol profiles. Other missions, GLI on ADEOS and POLDER scheduled for launch in the next few years will enhance to our ability to measure aerosol properties and forcing using different view and spectral conditions.

References

Alpert, P., Y. J. Kaufman, Y. Shay-El, D. Tanre, A. da Silva, S. Schubert, Y. H. Joseph, 1998; Quantification of Dust-Forced heating of the Lower Troposphere. *Nature*, 395, 367-370.

Boucher, O. and T.L. Anderson, General circulation model assessment of the sensitivity of direct climate forcing by anthropogenic sulfate aerosols to aerosol size and chemistry, J. Geophys. Res., 100, 26117-26134, 1995.

Boucher O., Tanré D., Estimation of the aerosol perturbation to the Earth's radiative budget over oceans using POLDER satellite aerosol retrievals, Geoph. Res. Let. 27, 1103-1106, 2000.

Charlson, R.J., S.E. Schwartz, J.M. Hales, R.D. Cess, J.A. Coakley, Jr., J.E. Hansen and D.J. Hofman, Climate forcing of anthropogenic aerosols, *Science*, 255, 423-430, 1992.

Chu, A., Y. J. Kaufman, L. A. Remer, B. N. Holben: Remote sensing of smoke from MODIS Airborne Simulator During SCAR-B Experiment. J. Geophys. Res.,103, 31,979-31,988, 1998.

Chu et al.,; 2000 in preparation

Fraser, R.S. and Y.J. Kaufman, the Relative Importance of Aerosol Scattering and Absorption in Remote Sensing, *IEEE J. Geosc. Rem. Sens.*, **GE-23,** 525-633, 1985.

Hansen, J., M. Sato and R. Ruedy, Radiative forcing and climate Response, J. Geophys. Res., 102, 6831-6864, 1997.

Haywood, J.M., V. Ramaswamy and L.J.Donner Goph. *Res. Let. 24*, 143-146, 1997.

Hignett, P., J.P. Taylor P.N. Francis and M.D. Glew, Comparison of observed and modeled direct aerosol forcing during Tarfox, , J. Geophys. Res.,104, 2279-2288, 1999

Hobbs, P. V., J. S. Reid, R. A. Kotchenruther, R. J. Ferek, and R. Weiss, Direct radiative forcing by smoke from biomass burning, *Science*, 275, 1776-1778, 1997.

Holben, B. N., T. F. Eck, I. Slutsker, D. Tanré, J. P. Buis, A. Setzer, E. Vermote, J. A. Reagan, Y. J. Kaufman, T. Nakajima, F. Lavenu, I. Jankowiak and A. Smirnov, 1998: AERONET-A federated instrument network and data archive for aerosol characterization, Rem. Sens. Environ., **66**, 1-16.

Holben, B.N., D. Tanre, A. Smirnov, T.F. Eck, I. Slutsker, Y.J. Kaufman, J. Van de Castle, A. Setzer, B. Markham, An emerging ground based aerosol climatology: Aerosol optical depth from AERONET, accepted to JGR, 2001.

Husar, R. B. , J. Prospero and L.L. Stowe, Patterns of tropospheric aerosols over the oceans, *J. Geophys. Res.* 102, 16,889 (1997).

Jacobson, M. Z., Strong radiative heating due to the mixing state of black carbon in atmospheric aerosols, *Nature*, 409, 695-697, 2001.

Kahn R., Banerjee P., McDonald D., Diner D. J., Sensitivity of multiangle imaging to aerosol optical depth and to pure-particle size distribution and composition over ocean, *J. Geoph. Res.*, 103, 32195-32213, 1998.

Kaufman, Y. J., 1987: Satellite Sensing of Aerosol Absorption. *J. Geoph. Res.*, 92, 4307-4317.

Kaufman, Y. J., P. V. Hobbs, V. W. J. H. Kirchhoff, P. Artaxo, L. A. Remer, B. N. Holben, M. D. King, E. M. Prins, D. E. Ward, K. M. Longo, L. F. Mattos, C. A. Noble, J.K.D. Spinhirne, Q. Ji, A. M. Thompson, J. F. Gleason, S. A.

Christopher, and S.-C. Tsay: The Smoke, Clouds and Radiation Experiment in Brazil (SCAR-B) *J. Geophys. Res., 103*, 31,783-31,808, 1998.

Kaufman, Y.J., B. N. Holben, S. Mattoo, D. Tanré, L.A. Remer, T. Eck and J. Vaughn: Aerosol radiative impact on spectral solar flux reaching the surface, derived from AERONET principal plane measurements, *J. Geoph. Res.*, in press, 2000.

Kaufman, Y.J., A. Smirnov, B. N. Holben and O. Dubovik, Background maritime aerosol: methodology to derive the optical thickness and scattering properties submitted to GRL, 2001.

Kaufman, Y. J., D. Tanré, L. Remer, E. Vermote, A. Chu, and B. N. Holben, Remote Sensing of Tropospheric Aerosol from EOS-MODIS Over the Land Using Dark Targets and Dynamic Aerosol Models. *J. Geoph. Res.*, 102, 17051-17067, 1997a.

Kaufman, Y. J., D. Tanré, A. Karnieli, and L.A. Remer: Re-evaluation of dust absorption and radiative forcing of climate using satellite and ground based remote sensing. Goph. Res. Let. in press, 2000b.

Kaufman, Y. J., A. Wald, L. A. Remer, B-.C. Gao, R.-R. Li and L. Flynn, Remote sensing of aerosol over the continents with the 2.2 μm channel. *IEEE TGARS*, 1286-1298, 1997b.

Kiehl, J. T., and B. P. Briegleb, The relative roles of sulfate aerosols and greenhouse gases in climate forcing, *Science, 260*, 311-314, 1993.

Martins, J. V., P. Artaxo, C. Liousse, J. S. Reid, P. V. Hobbs, and Y. J. Kaufman: Effects of black Carbon Content, Particle size, and, mixing on light absorption by aerosol particles from biomass burning in Brazil. *J. Geoph. Res.*, special issue on SCAR-B., *103*, 32,041-32,050, 1998.

Mishchenko. M.I., I.V. Geogdzhayev, B. Cairns, W.B. Rossow, and A.A. Lacis, Aerosol retrievals over the ocean by use of channels 1 and 2 AVHRR data: sensitivity analysis and preliminary results, *Appl. Optics, 38*, 7325-7341, 1999.

Nakajima, T. and A. Higurashi, 1998: A use of two channel radiances for an aerosol characterization from space, Geophys. Res. Lett., 25, 3815-3818.

Remer, L. A., Y. J. Kaufman, B. N. Holben, A. M. Thompson and D. McNamara, Tropical biomass burning smoke aerosol size distribution model. *J. Geoph. Res., 103*, 31,879-31,892, 1998.

Remer, L. A. and Y. J. Kaufman, 1998: Dynamical aerosol model: Urban/industrial aerosol., *J. Geophys. Res.*, 103, 13,859-13,871

Remer, L. A., D. Tanré, Y. J. Kaufman, C. Ichoku, S. Mattoo, R. Levy, D. A. Chu, B. N. Holben, J. V. Martins, and R.-R. Li and Z. Ahmad, Validation of MODIS Aerosol Retrieval Over Ocean, submitted to GRL, 2001

Russell P.B., J.M. Levington, P. Hignett, S. Kinne, et al., Aerosol induced radiative flux change off the coast of the United States mid Atlantic coast: Comparison of values calculated from the sunphotometer and in situ data with those measured by airborne pyranometer, J. Geophys. Res.,104, 2289-2308, 1999

Satheesh, S.K. and V. Ramanathan, Large differences in tropical aerosol forcing at the top of the atmosphere and Earth's surface, Nature, **405**, 60-63, 2000.

Satheesh, S.K., V. Ramanathan, L.J. Xu, J.M. Lobert, I.A. Podgorny, J.M. Prospero, B.N. Holben, and N.G. Loeb, A model for the natural and anthropogenic aerosols over the tropical Indian Ocean derived from Indian Ocean Experiment data, . *J. Geoph. Res., 104*, 27421-27440, 1999.

Tanré, D., M. Herman and Y.J. Kaufman: Information on aerosol size distribution contained in solar reflected radiances. *J. Geoph. Res., 101*, 19043-19060, 1996.

Tanré, D., Y. J. Kaufman, M. Herman and S. Mattoo, Remote sensing of aerosol over oceans from EOS-MODIS. *J. Geophys. Research* , 102, 16971-16988, 1997.

Tanré, D., L.R. Remer, Y.J. Kaufman, P.V. Hobbs, et al.: Retrieval of Aerosol Optical Thickness and Size Distribution Over Ocean from the MODIS Airborne Simulator during Tarfox, J. Geophys. Res.,104, 2261-2278, 1999.

Tanré, D., Y. J. Kaufman, B.N. Holben, B. Chatenet, A. Karnieli,F. Lavenu, L. Blarel, O. Dubovik, L.A. Remer, A. Smirnov: Climatology of dust aerosol size distribution and optical properties derived from remotely sensed data in the solar spectrum, JGR dust special issue submitted 2000.

Tegen, I., A.A. Lacis and I. Fung, The influence on climate forcing of mineral aerosols from disturbed soils, *Nature*, **380** ,419-422, 1996.

Table 1: Errors (%) in remote sensing of optical thickness (τ) and aerosol impact on the spectral flux (ΔF_{aer}) for 4 latitude zones over the ocean. The average solar zenith angle (θ_o) and scattering angle (Θ) are given. The errors in the sensor calibration, wind speed and aerosol model are computed for the accumulation mode and the coarse mode (See fig. 2 for details). Error in ΔF^S_{aer}, the aerosol effect on the integrated solar flux is also given for both size distributions. The bottom two lines give the maximum and minimum values of ΔF_{aer} and ΔF^S_{aer} for all the latitude zones.

	Average		Error (%) in Accum. Mode					Error (%) in Coarse mode				
Latitude (°)	<_o>	<_>	_	_Fae r 0.55 µm	_Fae r 0.86 µm	_Fae r 1.64 µm	_FSae r W/m 2	_	_Fae r 0.55 µm	ΔF_{aer} 0.86 µm	ΔF_{aer} 1.64 µm	ΔF^S_{aer} W/m²
60	60	103	21	3	-4	-33	1.1	-47	109	31	-16	6.7
30	33	118	17	0	-2	-16	1.2	-46	44	19	-18	4.1
0	19	127	14	3	-7	-28	1.4	-48	51	21	-19	3.9
-30	38	121	16	-1	-3	-17	1.2	-47	43	18	-18	3.9
-60	65	106	22	3	-4	-38	1.4	-49	162	34	-15	6.7
Maximum value			0.5	0.15	0.09	0.02	54	0.5	0.02	0.05	0.09	20
Minimum value			0.5	0.06	0.03	0.01	43	0.5	0.01	0.03	0.03	11

Figure captions:

Fig 1: Distribution of the scattering angle for MODIS scans during a month around the solar equinox, avoiding the glint region for glint angle ≥ 40°. Wider range of the scattering angle provides smaller sensitivity of the derived aerosol impact on the flux on the aerosol size distribution.

Fig 2: The error in the optical thickness (τ) and aerosol impact on the flux (ΔF_{aer}) over the ocean for an accumulation mode (top) and coarse mode (bottom), plotted as a function of the latitude. Calibration errors are introduced by multiplying the radiance by $(1+f_\lambda/100)$ where f_λ is: $f_{0.55}$=3%, $f_{0.66}$=2.5%, $f_{0.86}$=2%, $f_{1.24}$=1.5%, $f_{1.64}$=1%, $f_{2.1}$=0%. Model errors are introduced by increasing the real part of the refractive index by 0.1, increase in the accumulation mode (top) geometric radius r_g from r_g =0.06 μm to r_g =0.065 μm, and decrease in the coarse mode (bottom) from 0.50 μm to 0.45 μm. The wind speed was decreased from 6 to 4 m/s. For the accumulation mode the errors in the aerosol impact on the fluxes were significantly smaller for 0.55 and 0.86 μm than the errors in the optical thickness at 0.55 μm. For the coarse mode the errors in the aerosol effect on flux at 1.64 μm were significantly smaller than in the optical thickness.

Fig. 3: Instantaneous aerosol radiative forcing at the top of the atmosphere over the ocean, ΔF^s_{aer} - the difference in the reflected solar flux with and without the

aerosol (top), and the errors in the radiative forcing (bottom). Calculations are for solar zenith angle that corresponds to the local illumination conditions for the 10:30 am equatorial crossing time, for optical thickness of 0.5. A solar flux is assigned to each of the three MODIS bands used in the simulation of Fig. 2, based on the spectrum of transmitted solar energy. Results are shown for both the accumulation mode (r_g=0.06 μm) and the coarse modes (r_g=0.5 μm). The same uncertainties described in Fig 2 were applied to calculate the error in forcing.

Fig. 4: Large fire near Cuiaba on Aug. 25, 1995 observed from the ER-2 AVIRIS instrument (provided by Robert Green from JPL) during the SCAR-B experiment. The image is 10x20 km with 20 m resolution. The solar zenith angle is 36°. Top image: color composite that resembles the human vision (0.47 μm - blue, 0.55 μm - green and 0.66 μm - red), showing heavy smoke emitted from the fire. Bottom image – same, but for near-IR channels (2.1 μm - blue, 1.2 μm - green and 1.65 μm - red), with almost transparent smoke. Plot on the right: upward spectral radiance at the top of the atmosphere (normalized by the solar extraterrestrial flux $-F_o$) for several values of smoke optical thickness, τ. Smoke increases the radiance in the short wavelengths, (λ<0.7 μm) and has a mixed effect for longer wavelengths due to the vegetation brightness and smoke absorption of sunlight.

Fig. 5: Scatter plot of the measured spectrally integrated radiance reflected from the surface at nadir in flux units of (W/m^2) over the spectral range: 0.4-0.7 μm, and the estimated radiance: $\pi L(0.4\text{-}0.7\ \mu m) = 19 + 291 \cdot \rho_{2.13} - 44 \cdot \rho_{1.65}$ (W/m^2), where ρ is the apparent surface reflectance at the mid-IR channels. The zero values of $19 W/m^2$ is due to atmospheric scattering. The standard deviation in the error in F(0.4-0.7 μm) is 2-3 W/m^2, indicating that the surface contribution to the flux at the top of the atmosphere at 0.4-0.7 μm can be estimated from its properties at 1.65 and 2.13 μm with an error of 2-3 W/m^2

Fig. 6: Top: Integrated radiance over the spectral range of 0.4-0.7 μm, expressed in units of flux (W/m^2), as a function of the smoke optical thickness for Cuiaba, Parana and Alta Floresta. The optical thickness is given for wavelength of 0.64 μm. The data sets are for high sun of 28°-31°. Smoke optical thickness of 1.0 corresponds to an increase in the integrate radiance of 50-60 W/m^2. Bottom: The effect of smoke on the integrated radiance in the near IR (0.7-2.5 μm). The effect of smoke is observed as a function of the smoke optical thickness. The optical thickness is given for wavelength of 0.64 μm. Note that variation in the smoke optical thickness means also variation in the location and random variation in the surface properties. Change in the optical thickness of 1.0 corresponds to an increase in the integrate radiance of 2-8 W/m^2, in the cases shown.

Fig. 7: The smoke radiative forcing at the top of the atmosphere for the spectral range of 0.4-0.7 μm. Results are given as a function of the square root of the cosine of the solar zenith angle for three values of the smoke optical thickness.

Fig. 8: The solar diffuse spectral flux reaching the Earth surface at Alta Floresta, Brazil, as a function of the smoke optical thickness. The sky flux F is normalized by the solar extraterrestrial flux F_o and the cosine of the solar zenith angle, μ_o. Data are for the 1995 SCAR-B experiment. The symbols stand for fluxes derived from the AERONET data and the lines for the smoke model of Remer et al., (1998).

Fig. 9: The spectral optical thickness (top) and the corresponding spectral aerosol radiative forcing, normalized to the incoming solar flux $F_o\mu_o$ and to unit optical thickness at 0.55 μm – $\Delta F(\lambda)/F_o\mu_o\Delta\tau_{0.55}$. The data were collected by the MODIS Airborne Instrument during the Tarfox experiment in July 26, 1996 for solar zenith angle of 67° (Tanré et al., 1999). The different lines correspond to measurements during the Tarfox experiment for different fractions of the contribution of the accumulation mode to the optical thickness at 0.55 μm.

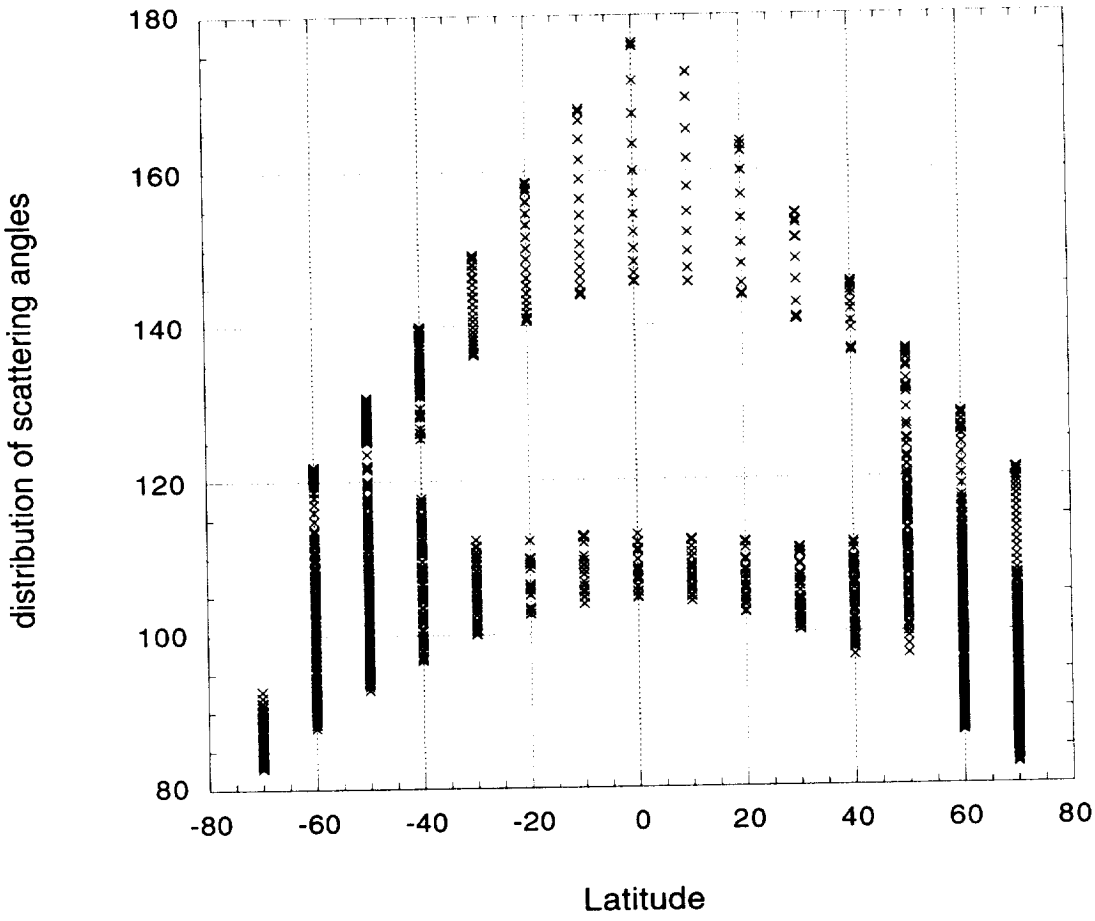

Fig 1: Distribution of the scattering angle for MODIS scans during a month around the solar equinox, avoiding the glint region for glint angle ≥ 40°. Wider range of the scattering angle provides smaller sensitivity of the derived aerosol impact on the flux on the aerosol size distribution.

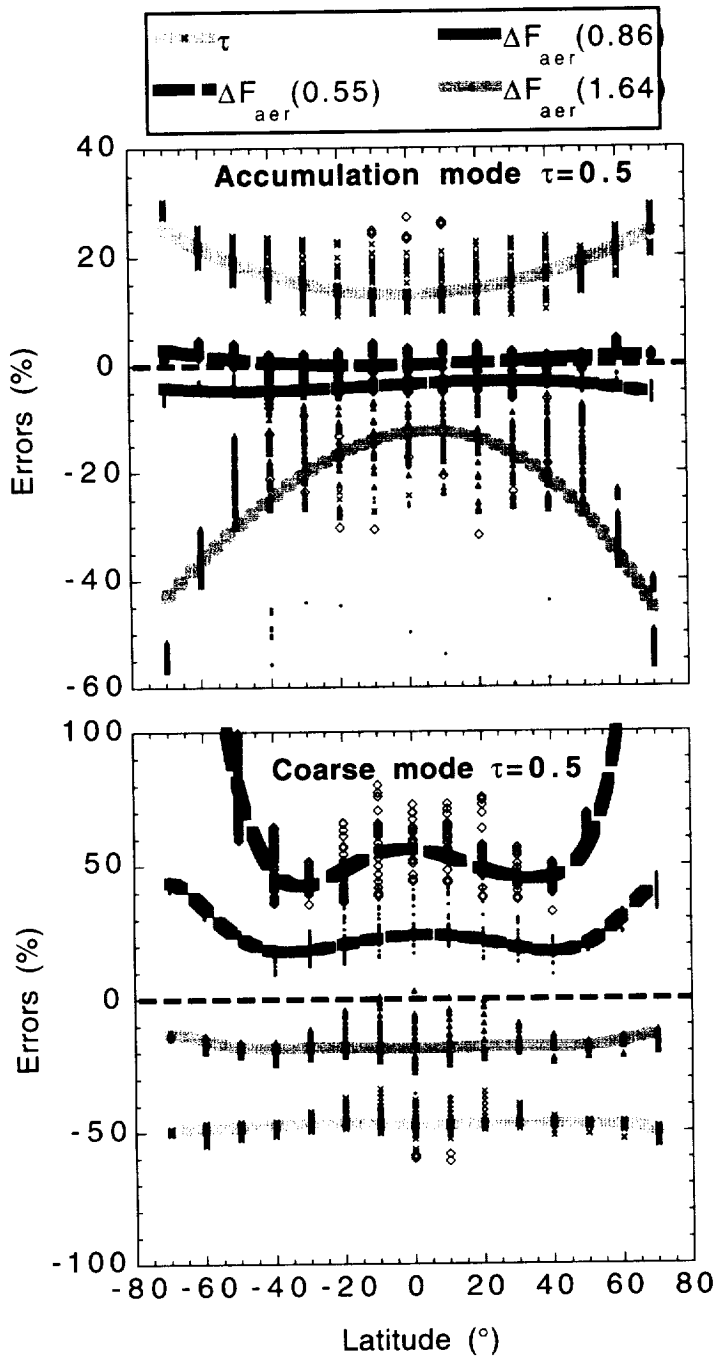

Fig 2: The error in the optical thickness (τ) and aerosol impact on the flux (ΔF_{aer}) over the ocean for an accumulation mode (top) and coarse mode (bottom), plotted as a function of the latitude. Calibration errors are introduced by multiplying the radiance by $(1+f_\lambda/100)$ where f_λ is: $f_{0.55}$=3%, $f_{0.66}$=2.5%, $f_{0.86}$=2%, $f_{1,24}$=1.5%, $f_{1.64}$=1%, $f_{2.1}$=0%. Model errors are introduced by increasing the real part of the refractive index by 0.1, increase in the accumulation mode (top) geometric radius r_g from r_g =0.06 μm to r_g =0.065 μm, and decrease in the coarse mode (bottom) from 0.50 μm to 0.45 μm. The wind speed was decreased from 6 to 4 m/s. For the accumulation mode the errors in the aerosol impact on the fluxes were significantly smaller for 0.55 and 0.86 μm than the errors in the optical thickness at 0.55 μm. For the coarse mode the errors in the aerosol effect on flux at 1.64 μm were significantly smaller than in the optical thickness.

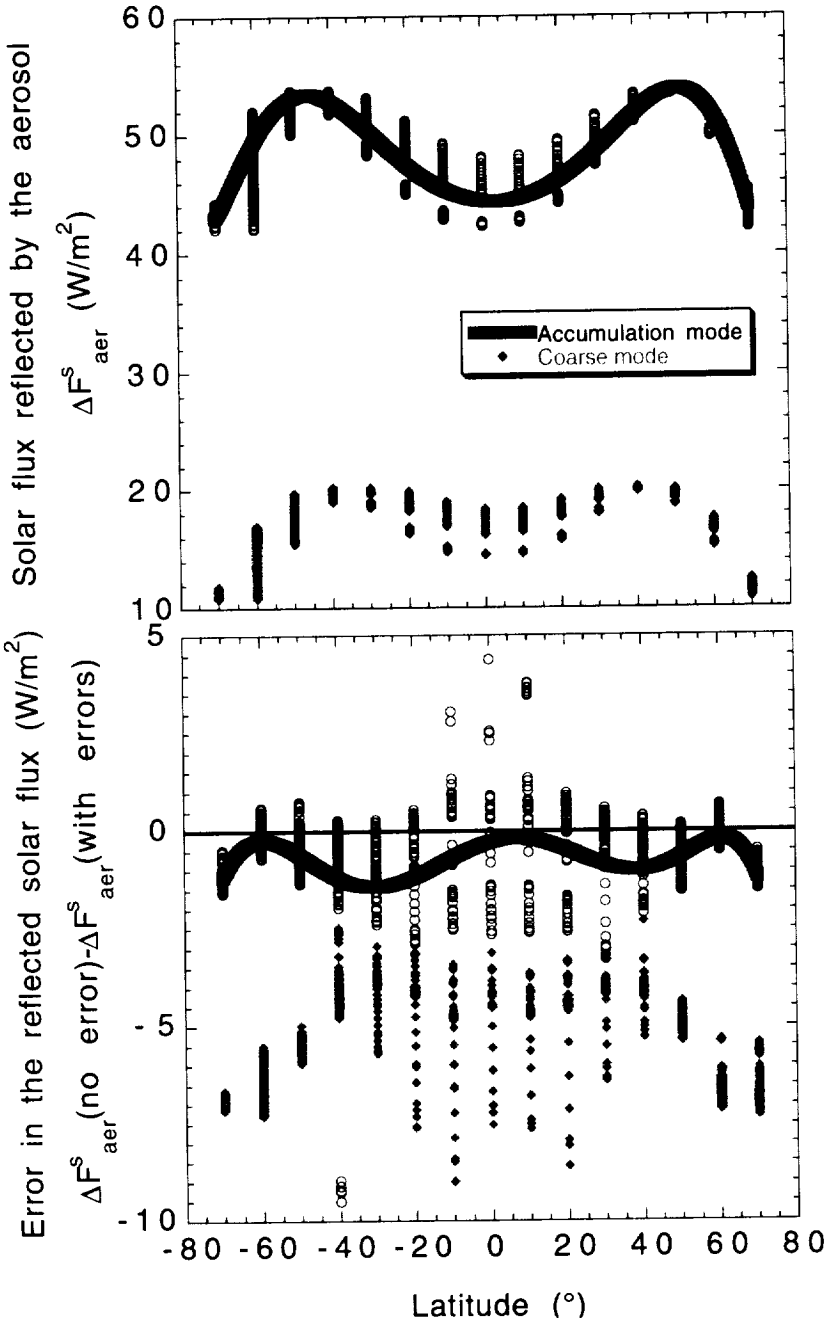

Fig. 3: Instantaneous aerosol radiative forcing at the top of the atmosphere over the ocean, ΔF^s_{aer} - the difference in the reflected solar flux with and without the aerosol (top), and the errors in the radiative forcing (bottom). Calculations are for solar zenith angle that corresponds to the local illumination conditions for the 10:30 am equatorial crossing time, for optical thickness of 0.5. A solar flux is assigned to each of the three MODIS bands used in the simulation of Fig. 2, based on the spectrum of transmitted solar energy. Results are shown for both the accumulation mode (r_g=0.06 μm) and the coarse modes (r_g=0.5 μm). The same uncertainties described in Fig 2 were applied to calculate the error in forcing.

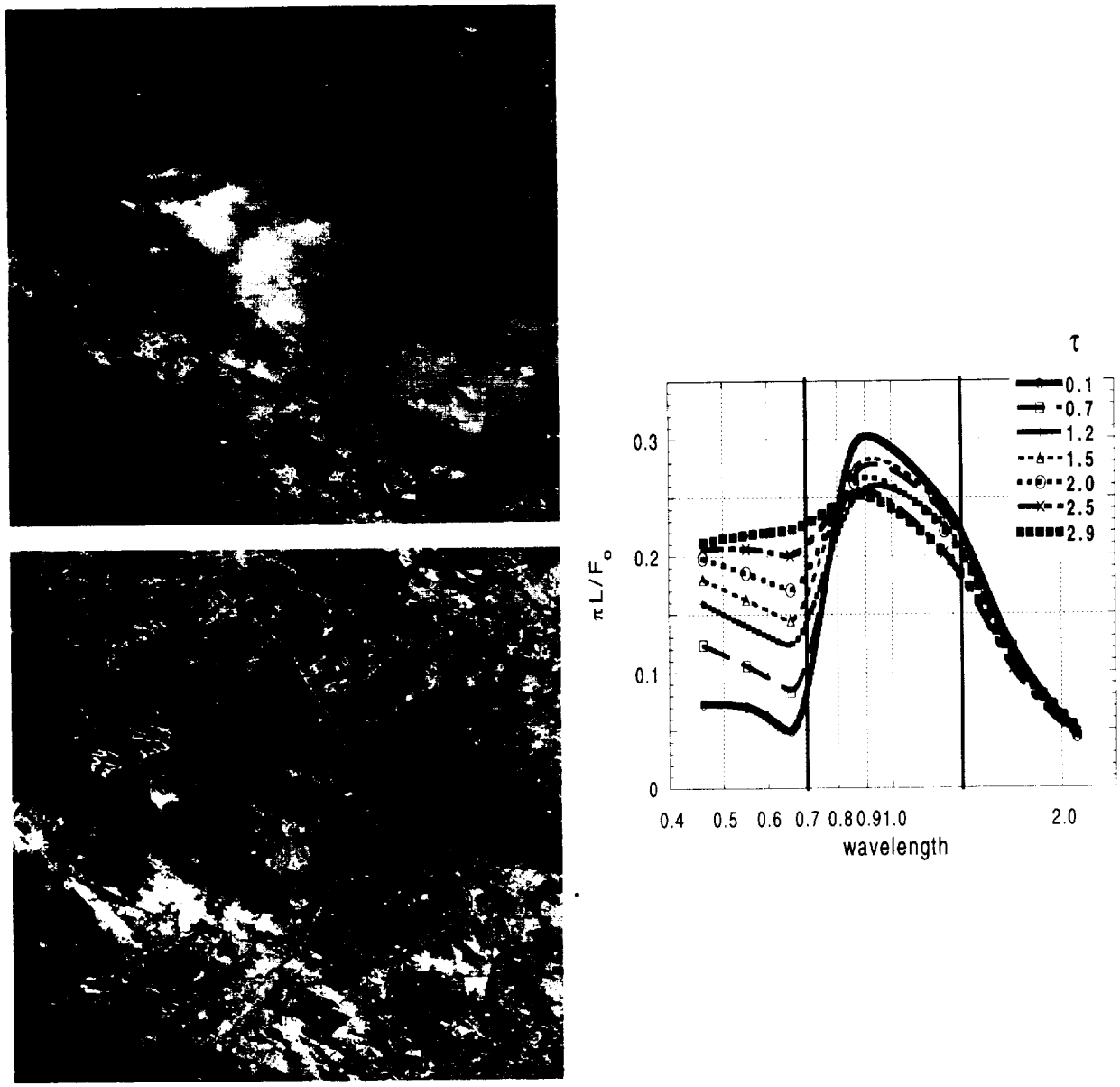

Fig. 4: Large fire near Cuiaba on Aug. 25, 1995 observed from the ER-2 AVIRIS instrument (provided by Robert Green from JPL) during the SCAR-B experiment. The image is 10x20 km with 20 m resolution. The solar zenith angle is 36°. Top image: color composite that resembles the human vision (0.47 μm - blue, 0.55 μm - green and 0.66 μm - red), showing heavy smoke emitted from the fire. Bottom image – same, but for near-IR channels (2.1 μm - blue, 1.2 μm - green and 1.65 μm - red), with almost transparent smoke. Plot on the right: upward spectral radiance at the top of the atmosphere (normalized by the solar extraterrestrial flux $-F_o$) for several values of smoke optical thickness, τ. Smoke increases the radiance in the short wavelengths, (λ<0.7 μm) and has a mixed effect for longer wavelengths due to the vegetation brightness and smoke absorption of sunlight.

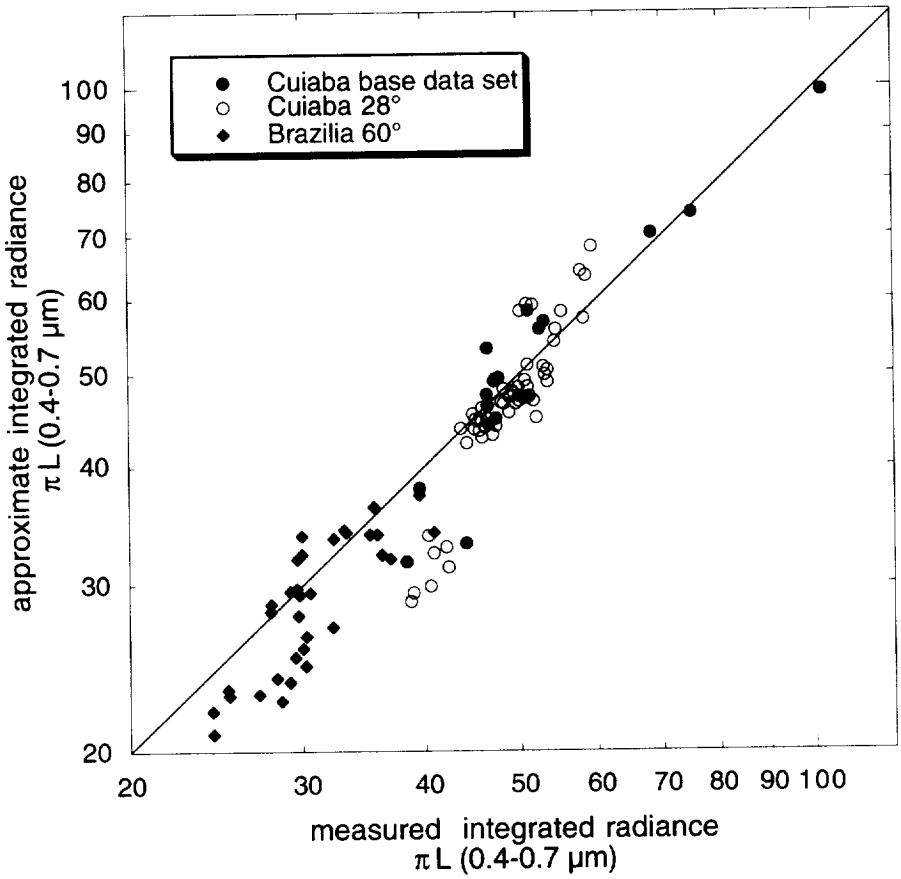

Fig. 5: Scatter plot of the measured spectrally integrated radiance reflected from the surface at nadir in flux units of (W/m^2) over the spectral range: 0.4-0.7 μm, and the estimated radiance: $\pi L(0.4\text{-}0.7\ \mu m) = 19 + 291 \cdot \rho_{2.13} - 44 \cdot \rho_{1.65}$ (W/m^2), where ρ is the apparent surface reflectance at the mid-IR channels. The zero values of $19 W/m^2$ is due to atmospheric scattering. The standard deviation in the error in F(0.4-0.7 μm) is 2-3 w/m^2, indicating that the surface contribution to the flux at the top of the atmosphere at 0.4-0.7 μm can be estimated from its properties at 1.65 and 2.13 μm with an error of 2-3 w/m^2

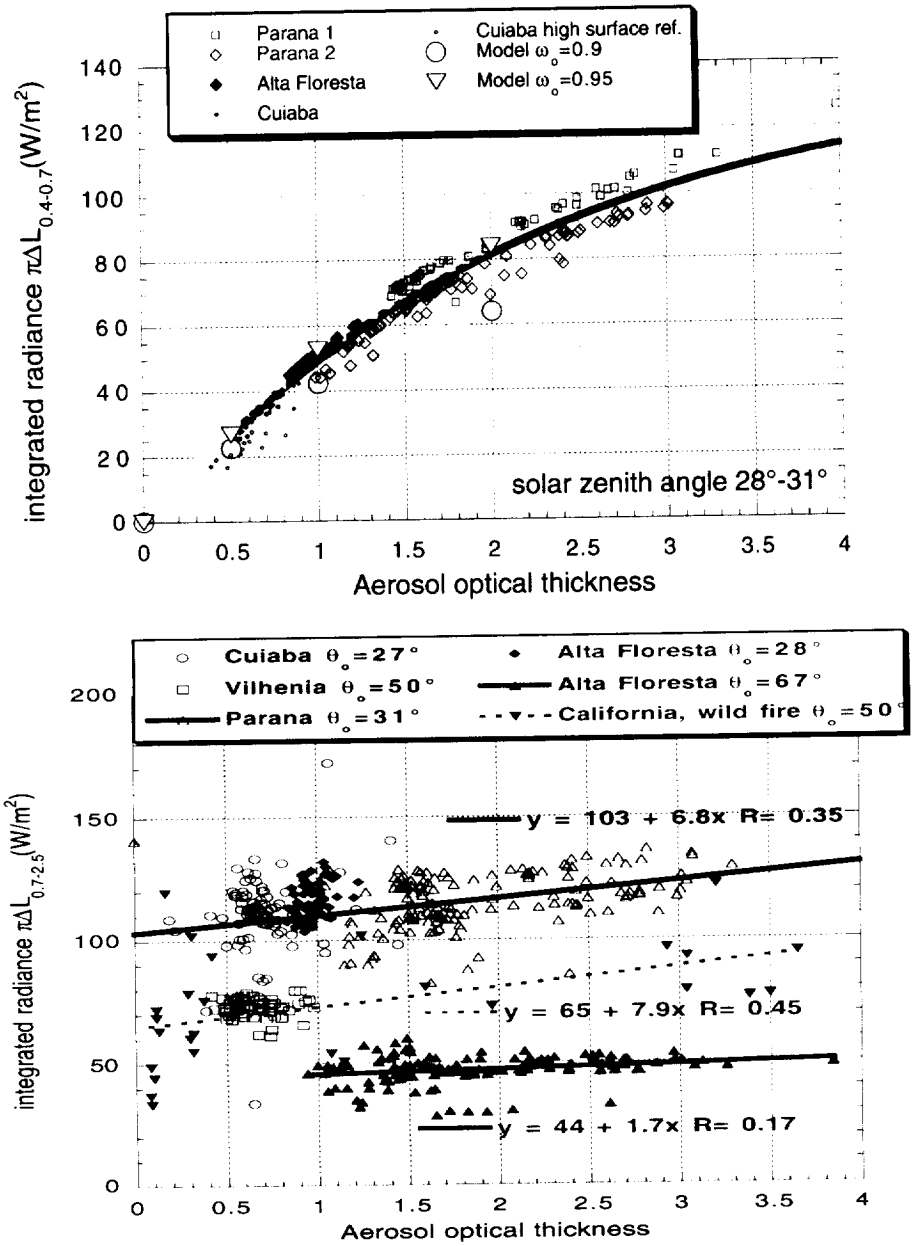

Fig. 6: Top: Integrated radiance over the spectral range of 0.4-0.7 μm, expressed in units of flux (W/m^2), as a function of the smoke optical thickness for Cuiaba, Parana and Alta Floresta. The optical thickness is given for wavelength of 0.64 μm. The data sets are for high sun of 28°-31°. Smoke optical thickness of 1.0 corresponds to an increase in the integrate radiance of 50-60 W/m^2. Bottom: The effect of smoke on the integrated radiance in the near IR (0.7-2.5 μm). The effect of smoke is observed as a function of the smoke optical thickness. The optical thickness is given for wavelength of 0.64 μm. Note that variation in the smoke optical thickness means also variation in the location and random variation in the surface properties. Change in the optical thickness of 1.0 corresponds to an increase in the integrate radiance of 2-8 W/m^2, in the cases shown.

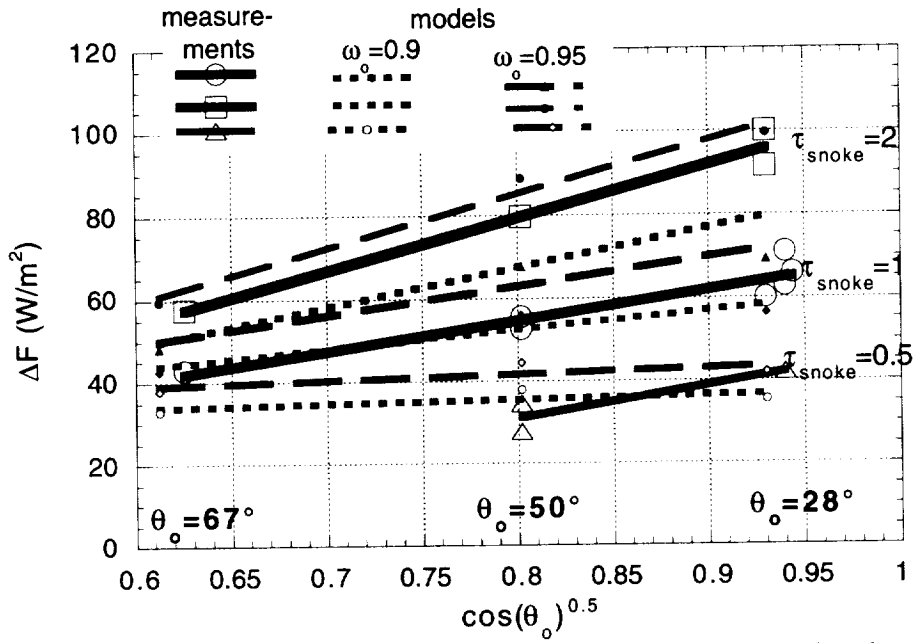

Fig. 7: The smoke radiative forcing at the top of the atmosphere for the spectral range of 0.4-0.7 μm. Results are given as a function of the square root of the cosine of the solar zenith angle for three values of the smoke optical thickness.

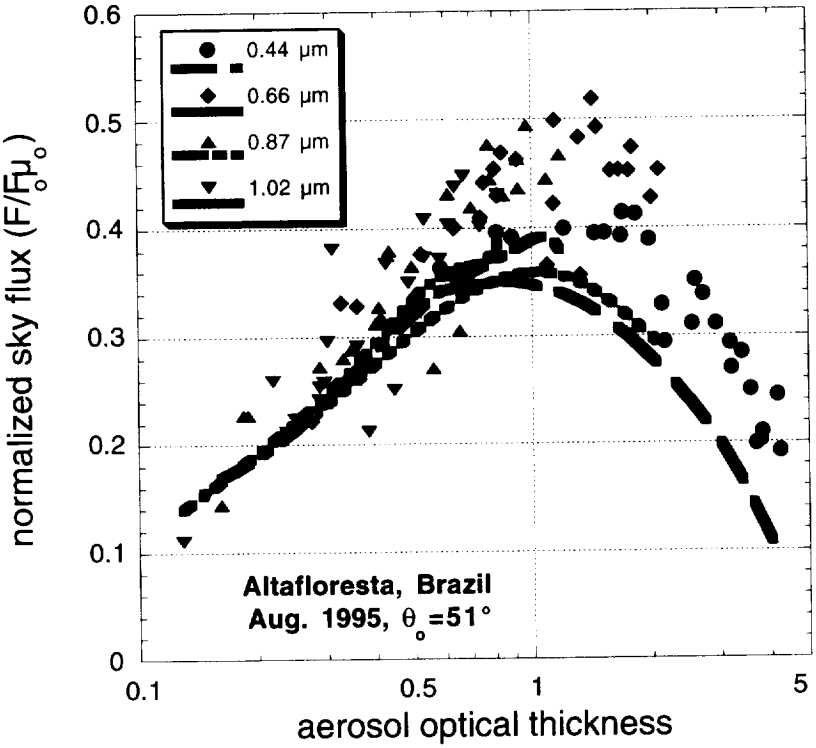

Fig. 8: The solar diffuse spectral flux reaching the Earth surface at Alta Floresta, Brazil, as a function of the smoke optical thickness. The sky flux F is normalized by the solar extraterrestrial flux F_o and the cosine of the solar zenith angle μ_o. Data are for the 1995 SCAR-B experiment. The symbols stand for fluxes derived from the AERONET data and the lines for the smoke model of Remer et al., (1998).

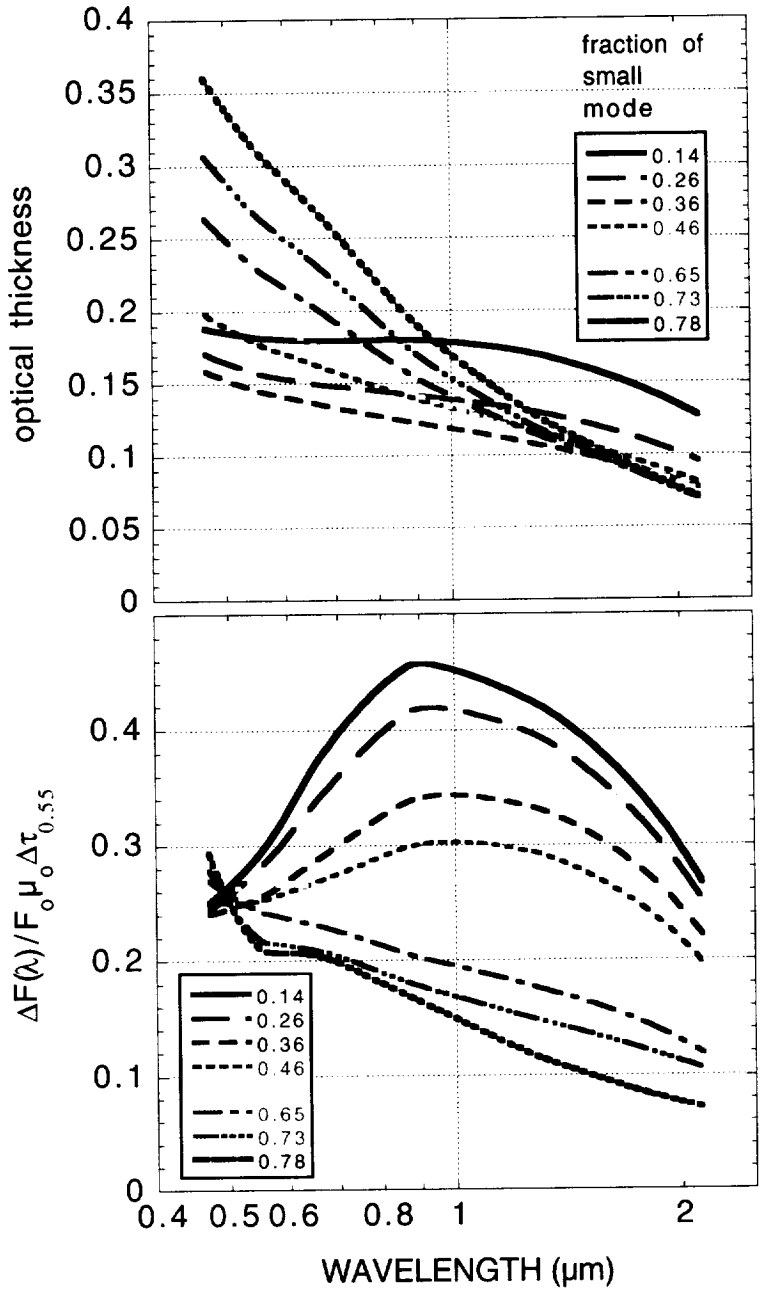

Fig. 9: The spectral optical thickness (top) and the corresponding spectral aerosol radiative forcing, normalized to the incoming solar flux $F_o\mu_o$ and to unit optical thickness at 0.55 μm – $\Delta F(\lambda)/F_o\mu_o\Delta\tau_{0.55}$. The data were collected by the MODIS Airborne Instrument during the Tarfox experiment in July 26, 1996 for solar zenith angle of 67° (Tanré et al., 1999). The different lines correspond to measurements during the Tarfox experiment for different fractions of the contribution of the accumulation mode to the optical thickness at 0.55 μm.